Clinical implementation of PLANET®Dose for dosimetric assessment after [177Lu]Lu-DOTA-TATE : comparison with Dosimetry Toolkit® and OLINDA/EXM® V1.0

Lore Santoro (ore.santoro@icm.unicancer.fr)
Institut regional du Cancer de Montpellier https://orcid.org/0000-0002-8935-1450
Laurine Pitalot
Institut regional du Cancer de Montpellier
Dorian Trauchessec
Institut regional du Cancer de Montpellier
Erick Mora-Ramirez
Universidad de Costa Rica
Pierre-Olivier Kotzki
Institut regional du Cancer de Montpellier
Manuel Bardiès
INSERM UMR 1037
Emmanuel Deshayes
Institut regional du Cancer de Montpellier

Original research

Keywords: Dosimetry workstation, Peptide Receptor Radionuclide Therapy, [177Lu]Lu-DOTA-TATE, 3D calibration factor, MIRD, voxel-based dosimetry

Posted Date: September 11th, 2020

DOI: https://doi.org/10.21203/rs.3.rs-36998/v2

Version of Record: A version of this preprint was published on January 4th, 2021. See the published version at https://doi.org/10.1186/s13550-020-00737-8.

Abstract

Background: The aim of this study was to compare a commercial dosimetry workstation (PLANET®Dose) and the dosimetry approach (GE Dosimetry Toolkit® and OLINDA/EXM® V1.0) currently used in our department for quantification of the absorbed dose in organs at risk after peptide receptor radionuclide therapy with [177Lu]Lu-DOTA-TATE.

Methods: An evaluation on phantom was performed to determine the SPECT calibration factor variations over time and to compare the Time Integrated Activity Coefficients (TIACs) and absorbed doses obtained with the two tools. Then, the two tools were used for dosimetry evaluation in 21 patients with neuroendocrine tumours after the first and second injection of 7.2 ± 0.2 GBq of [177Lu]Lu-DOTA-TATE (40 dosimetry analyses with each software). SPECT/CT images were acquired at 4h, 24h, 72h and 192h after [177Lu]Lu-DOTA-TATE injection and were reconstructed using the Xeleris software (General Electric). The liver, spleen and kidney masses, TIACs and absorbed doses were calculated using i) GE Dosimetry Toolkit® (DTK) and OLINDA/EXM® V1.0 and ii) the Local Deposition Method (LDM) or Dose voxel-Kernel convolution (DK) on PLANET®Dose.

Results: With the phantom, the 3D calibration factors showed a slight variation (0.8% and 3.3%) over time and TIACs of 225.19h and 217.52h were obtained with DTK and PLANET®Dose, respectively. In patients, the root mean square deviation value was 8.9% for the organ masses, 8.1% for the TIACs, and 9.1 and 7.8% for the absorbed doses with LDM and DK, respectively. The Lin's concordance correlation coefficient was 0.99 and the Bland-Altman plot analysis estimated that the difference of absorbed dose values between methods ranged from -0.75 Gy to 0.49 Gy, from -0.20 Gy to 0.64 Gy and from -0.43 to 1.03 Gy for approximately 95% of the 40 liver, kidneys and spleen dosimetry analyses. A difference of 2.2% was obtained between the absorbed doses to organs at risk calculated with LDM and DK.

Conclusions: The absorbed doses to organs at risk obtained with the new workstation are concordant with those calculated with the currently used software and in agreement with the literature. These results validate the use of PLANET®Dose in clinical routine for patient dosimetry after targeted radiotherapy with [177Lu]Lu-DOTA-TATE.

Background

The role and relevance of dosimetry in targeted radionuclide therapy is a matter of hot debates (1–3). Dosimetry applications are expanding and the number of nuclear medicine departments performing patient dosimetry, especially in peptide receptor radionuclide therapy for neuroendocrine tumours (4), is growing thanks to the solid collaboration between nuclear medicine physicians, medical physicists and nuclear medicine technologists (3).

Dosimetry procedures can be implemented to impact the treatment, i.e. personalise radiopharmaceutical administration (administered activity modulation). This is obviously an appealing goal – that requires the preliminary appraisal of AD effect correlations (5). Even when the immediate objective is not to modulate

the administered activity based on dosimetric findings, the documentation of the therapeutic procedure delivered is recommended by European Directives (6).

Two global approaches can be identified, depending on the clinical aim: Organ at risk (OAR) dosimetry is designed to insure that the therapeutic procedure induces no harm to the patient. It may, or not, be used to modulate activity (As High As Safely Attainable - AHASHA) (7). Tumour dosimetry is more challenging in nuclear medicine therapy than in external beam radiotherapy. The reason is the difficulty to identify and delineate multiple tumours of variable size and affinity for the radiopharmaceutical, as is often observed in the clinics. This may be a reason why OAR dosimetry is more often observed than tumour dosimetry.

Dosimetry requires the determination of pharmacokinetics, i.e. radioactive source assessment in space (within the patient) and time (from administration to excretion). This yields the number of radioactive decays in patient's tissues, the Time Integrated Activity (TIA) according to the MIRD nomenclature (8).

Then, from the distribution of the number of decays in the patient, the emitted energy is easy to derive, as the emitted energy per decay is well known for most radioactive isotopes used in nuclear medicine. Computing the absorbed dose requires the characterisation of the propagation of radiations in tissues. This can be obtained from precomputed tables established for patient models (the S values or absorbed doses in the target per decay in the source – in $Gy.Bq^{-1}.s^{-1}$ or equivalent). S values have been computed for several radionuclides (9–11) and are integrated in software packages, such as OLINDA/EXM (12) or IDAC-Dose (13). It is also possible to personalize the calculation by adjusting the S values to the organ mass (14).

The patient specific calculation of the absorbed dose can also be performed, and requires the characterisation of the radiation propagating medium (usually from patient's CT) and the implementation of radiation transport and energy scoring algorithms. For the later, 3 broad categories can be designed:

- When spatial samplings (voxel dimensions) are small compared to radiation range, it is possible to assume that most emitted energy is absorbed locally (15).
- For homogeneous media, as radiation transport and energy deposition depend only on the distance to the source, and thanks to the superposition principle it is possible to implement convolution approaches (16–18).
- Then for heterogeneous media and when radiation range is high when compared to spatial sampling it is necessary to model explicitly radiation transport using Monte Carlo codes (19), even though the very long computing times required are a limitation to their use in clinical routine.

In the clinic, many medical teams have developed their own methodology using the tools available in their department and according to their own organizational possibilities (20–22), and specific dosimetry software and programs have been developed and implemented locally (23–27). However, the legislation on Medical Devices restricts their use to clinical studies. In order to use a software in clinical routine, it

must have the CE marking, and this orients towards commercial packages, as getting CE marking is usually beyond academic structure missions/capabilities.

Commercial software tools are increasingly available. In a previous article we evaluated some commercial packages available on the market (28). An updated table (Table 1) is presented below, but is subjected to changes as the field is evolving quickly. Only software that have CE marking are presented (STRATOS from the Philips research station Imalytics has therefore been removed from the list), and it must be stressed that some features that are under development may not have been approved yet.

In our department, dosimetry is integrated in the clinical routine for the management of patients with neuroendocrine tumours treated by peptide receptor radionuclide therapy with [177Lu]Lu-DOTA-TATE. The first dosimetry analyses of OARs were performed using the combination Dosimetry Toolkit® (GE Healthcare, Milwaukee, USA) and OLINDA/EXM® V1.0 for TIA assessment and organ-level dose calculation, respectively (29). Recently, our department acquired PLANET®Dose (DOSIsoft SA, Cachan, France), a new CE marked commercial dosimetry workstation. The initial motivation for changing was to use a vendor-neutral solution to support multicentric trials and to be able to implement central dosimetric processing.

Before implementing this new device in clinical routine, our goal was to compare it with our internal reference, using similar parameters in terms of segmentation, registration, and time activity curve fitting. The purpose of this work was to validate PLANET®Dose by comparing the results on phantom (calibration factors, time activity curve) and in patients (mean AD to OARs, TIACs and organ volumes), but also to assess if the dosimetric results obtained previously with Dosimetry Toolkit® and OLINDA/EXM® V1.0 in our department would be consistent with results obtained with PLANET®Dose.

Material And Methods

Dosimetry software platforms

The characteristics of the dosimetry software platforms used in this study are presented in Table 2.

PLANET®Dose is a treatment planning system from DOSIsoft. The calibration procedure is left to the user's discretion and a CF (in $Bq.count^{-1}$) is required. This dosimetry platform does not reconstruct SPECT/CT data, but accepts reconstructed data in DICOM format from all devices. It provides multi-time point registration (rigid and elastic), organ segmentation (manual and automatic), and TIAC calculation with a wide choice of interpolation methods of the time-activity curve (linear, trapezoidal, mono-, X-, bi-, tri-exponential …). The mean AD can be calculated with or without media density correction, using either the local energy deposition (LDM) or convolution of dose voxel kernels (DK) (15,32,33) (Fig. 1b).

For this study, the segmentation, registration and TIAC steps were carried out on PLANET®Dose with restricted parameters, similar to those defined in DTK.

Dosimetry imaging protocol

All imaging acquisitions were performed with a SPECT/CT Discovery NM/CT 670 apparatus (General Electric [GE] Healthcare), including a BrightSpeed 16 CT scanner and a 3/8-inch NaI(Tl) crystal, according to the previously described acquisition protocol (29). Briefly, nuclear medicine images were acquired using a medium-energy general purpose parallel-hole collimator. A 20% energy window centered on the 208 keV photopeak and a 10% scatter correction window centered on 177 keV were applied. NM acquisitions were realized using a body contour option, rotation of 180° per detector, total of 60 projections and 45s each. For attenuation correction, CT images were acquired (120 kV, automatic mA regulation with a max at 200 mA, noise index at 6.43, slice thickness of 5 mm, rotation time of 0.8 s, pitch 1.375, 512x512 pixels matrix), with standard reconstruction.

The application “Preparation for Dosimetry Toolkit” was used for SPECT/CT image reconstruction for both dosimetry approaches. The Ordered Subset Expectation Maximization iterative reconstruction algorithm was used with 6 iterations and 10 subsets, attenuation, scatter, recovery resolution corrections and a Gaussian post-filter of 0.11 cm.

Phantom study

Calibration factor, Time Integrated Activity Coefficient

A NEMA IEC body phantom (Body Phantom NU2-2001/2007) containing two bottles of 250 mL filled with 200 mL of 82.2 ± 4.1 MBq [177Lu]Lu-DOTA-TATE was used. The intention was to obtain a geometry close to that of the kidneys. The background was filled with non-radioactive water. SPECT/CT images were acquired once at different time points to evaluate CF variations over time. The CF was estimated using one of the two bottles (Fig. 2).

Dosimetry Toolkit. A CT rigid registration centred on the full phantom was performed with “Preparation for Dosimetry Toolkit”. Then, using the “Dosimetry Toolkit” application, an isocontour representing a volume of 200 mL was automatically segmented on the first NM image and was replicated for the images at 24h, 72h, 120h and 216h. For each time-point, the segmented volume was kept constant, but its position was adjusted on the CT image by translation or rotation. To determine the CF in counts.s^{-1}.MBq^{-1} at each time point, the number of events in the volume was divided by the acquisition time provided by the DICOM data (2700s) and by the activity. For radioactivity decay correction, a physical half-life of 6.647 days (34) was applied and the activity at each acquisition time was corrected from the phantom preparation time. The computed CF was the mean of the CFs at the different time points. To obtain the time-activity curve fitted by a mono-exponential function and the TIAC (h), information about the radionuclide and the previously calculated CF were entered in the appropriate interface.

PLANET®Dose. A CT rigid registration centred on the bottle was performed with PLANET®Dose. Similarly, an isocontour representing a volume of 200 mL was automatically segmented on the first functional image and was rigidly propagated to the other time point images. The segmented volume was

maintained over time. To determine the CF in Bq.count^{-1} at each time point, the number of events in the volume was divided by the activity in Bq, by taking into account the radioactivity decay. The computed CF was the mean of the CFs at the different time points. A mono-exponential fitting function, similar to the DTK approach, was used to calculate the TIAC (h).

In the phantom study, as a mono-exponential activity decay occurred due to the radioisotope physical half-life, the TIA, , and the TIAC, , were estimated as follows (35):

$$\tilde{A} = \left[\frac{A_0 \times T_{eff} \times f}{ln2}\right] \quad \text{and} \quad \tau = \left[\frac{1}{\ln 2}\right] \times T_{eff} \times f = 230.15\ h$$

where A_0 is the injected activity, f is the bound activity fraction (1 in this case), and $T_{eff} = T_R$ is ^{177}Lu physical half-life (6.647 days) (34).

The theoretical τ of 230.15h was considered as the reference TIAC and was compared to the values obtained with the two dosimetry platforms.

Mean absorbed dose

The mean AD was calculated using 3 approaches presented in Fig 1:

- The GE DTK approach uses TIAC provided by DTK, entered in OLINDA/EXM® V1.0 to derive average absorbed doses to tissues/organs (Fig. 1a).
- The PLANET®Dose approach uses reconstructed images (Preparation for DTK) and full processing (registration, segmentation, TIAC and absorbed dose calculation using LDM and DK methods, with and without density correction) on PLANET®Dose (Fig. 1b).
- The third approach is similar to the former, but stops at the TIAC step to compute absorbed doses with OLINDA (Fig. 1c) for a kidney mass adjusted to 200 g.

Similarly, by knowing the theoretical TIAC of the radionuclide in the phantom, a theoretical absorbed dose was calculated using OLINDA/EXM V1.0 for a kidney mass adjusted to 200 g, and this value was compared to those obtained with the TIACs from PLANET®Dose and from DKT in OLINDA/EXM V1.0.

Clinical study

Patients and treatment

Twenty-one patients (5 women and 16 men; median age 68 years, range 41 to 82 years) with a neuroendocrine tumour and treated with [177Lu]Lu-DOTA-TATE, Lutathera® (Advanced Accelerator Applications, Saint Genis Pouilly, France) were evaluated (Table 3). The treatment consisted in 7.2 ± 0.2 GBq activity (four infusions in total) injected every 8 weeks. Amino acids (lysine + arginine) were administered concomitantly to ensure renal protection by reducing tubular reabsorption of the radiolabelled peptides. All patients were hospitalized in specialized radioprotection rooms for 24h after

injection. Patients were then released and had to come back for further imaging sessions. OAR dosimetry (liver, kidneys and spleen) was performed after the first and second infusion of [177Lu]Lu-DOTA-TATE. Dosimetry data after cycle 1 were not evaluable in one patient and another patient died before the second infusion. In total, 40 dosimetry analyses were performed with each dosimetry platform.

The study was approved by the local ethical review board.

Dosimetry workflow

The dosimetry workflow for the two platforms is presented in Table 4. SPECT/CT images were acquired at 4h, 24h, 72h and 192h after infusion. For some patients, due to health problems, technical issues or calendar reasons, SPECT/CT images were acquired at only three time points after injection. As dosimetry for the first 2 cycles of the therapy is performed routinely in our department, currently with DTK+OLINDA, we performed a retrospective additional analysis with PLANET®Dose of clinical data already available.

Reference dosimetry method (Fig. 1a). For infusion 1 and 2, after the last SPECT/CT image acquisition at 192h, all SPECT/CT data were loaded on the “Preparation for Dosimetry Toolkit” application. Imaging data were reconstructed and an automatic rigid registration between CT scans was performed. The results were loaded on the “Dosimetry Toolkit” application. The OARs (liver, kidneys and spleen) were manually segmented using the CT images collected at 4h post-injection, and then rigidly propagated to the 24h, 72h, and 192h images. For each time point, the segmented volume was maintained, but sometimes it was adjusted by translation or rotation. For the OARs considered in our study the partial volume effect correction was considered negligible. Information about the administered activity, the date and time of administration, the radionuclide and the CF (in $counts.s^{-1}.MBq^{-1}$) were entered. To obtain the TIAC, the time-activity curves were fitted using a mono-exponential function, the only fitting model available in the “Dosimetry Toolkit” application. Then, the TIAC values were exported to OLINDA/EXM® V1.0 to calculate the OAR absorbed doses. The organ masses included in this software were determined from the organ volume defined on the CT images using “Dosimetry Toolkit” and the biological tissue density (1.06 $g.cm^{-3}$ for liver and spleen; 1.05 $g.cm^{-3}$ for kidney).

PLANET®Dose (Fig. 1b). The transversal slices reconstructed using the “Preparation for Dosimetry Toolkit” application and the corresponding CT images were uploaded on PLANET®Dose. A study was created for each organ to simulate the Dosimetry Toolkit registration method. The rigid and automatic registration was centred on the OARs and then saved. The first CT scan was manually segmented and then propagated rigidly to the others. The volume of each OAR remained constant at all time points. As mentioned above, the partial volume effect correction was considered negligible for the OARs studied.

Information about the administered activity, the date and time of administration, the radionuclide and the CF (in $Bq.counts^{-1}$) was entered. The time-activity curve was fitted using a similar approach as the one used in DTK (i.e. mono-exponential function) to provide the TIAC (h) and the TIA (MBq.s). The mean absorbed doses were calculated using the LDM and DK methods, with correction of density.

Additionally to the relative difference (in %), the root mean-square deviation (RMSD) of organ masses, TIACs and absorbed doses per cycle obtained with PLANET®Dose and DTK/OLINDA (taken as reference) was calculated as follows:

$$RMSD = \sqrt{\frac{\sum_i \left[\frac{\left(X_{planetdose\ i} - X_{DTK\ Olinda\ i}\right)}{X_{DTK\ Olinda\ i}}\right]^2}{number\ of\ dosimetry\ analysis}}$$

Where $X_{(i)}$ was organ masses, TIACs or ADs obtained for the dosimetry analysis i

For the AD, the results obtained using the LDM and DK methods from PLANET®Dose, with density correction, were compared with those obtained using DTK+OLINDA/EXM V1.0.

To evaluate independently the absorbed dose calculation methods, the TIACs from PLANET®Dose were exported to OLINDA/EXM® V1.0. The organ masses included in the software were those determined from the organ volume defined on the CT images using PLANET®Dose and the biological tissue density. The mean AD obtained with PLANET®Dose (density correction) and with “PLANET®Dose + OLINDA/EXM® V1.0” (taken as reference) were compared (Fig. 1c).

Concordance evaluation

The Lin’s concordance correlation coefficient (36) was used to evaluate the agreement between PLANET®Dose LDM and the reference method (DTK+OLINDA) and then, between PLANET®Dose LDM and PLANET®Dose + OLINDA. These analyses were performed using the values for all patients and organs after the two infusions. In addition, absolute differences between the ADs obtained with the two approaches with regard to the average value of the two were assessed for each organ using the Bland-Altman plot analysis (37). The 95% limits of agreement, from -1.96 to +1.96 SD, were calculated for each organ.

The paired Student’s *t*-test was used to compare the OAR absorbed doses calculated with DTK+OLINDA and PLANET®Dose LDM (n=40). This analyse was performed using the mean values for all patients and organs after the two infusions.

Results

Phantom-based study

CF, TIAC and absorbed dose

SPECT/CT CF of 5.60 ± 0.04 counts.s^{-1}.MBq^{-1} and 5.53 ± 0.19 counts.s^{-1}.MBq^{-1} are obtained with Dosimetry Toolkit and PLANET®Dose, respectively. These values do not vary significantly over time (0.8%

and 3.3% of variation, respectively) (Fig. 3). For PLANET®Dose, the CF is converted into 67 ± 2.2 $Bq.counts^{-1}$ as expected by the software.

These CF values are used in the clinical study to calculate the time activity curves and TIACs for liver, kidneys, and spleen.

TIACs of 217.52h and 225.19h are obtained with DTK and PLANET®Dose, respectively. These values show a deviation of -5.5% and -2.2% relative to the theoretical residence time of 230.15h. The mono-exponential adjustment curves obtained with Dosimetry Toolkit and PLANET®Dose are presented in Table 5.

The AD value of 7.98 Gy determined by OLINDA/EXM V1.0 from the TIACs calculated with PLANET®Dose is close to the value obtained by PLANET®Dose with DK and density correction (-1.8%), and with LDM and density correction (-4.3%). A difference of 2.2% between the ADs calculated by PLANET®Dose with LDM and DK is observed, and a deviation of 6.7% between the ADs calculated with and without density correction for both methods.

Clinical results

Platform comparison

The mean organ masses, TIACs and ADs for liver, kidneys and spleen obtained using each dosimetry platform are summarized in Table 6a. The relative differences of the organ mass values and TIACs between DTK+OLINDA/EXM® V1.0 (the reference) and PLANET®Dose are compared and presented in Table 6b. These results highlight RMSD values within 10% for organ mass values and TIACs, excepted for spleen with a value of 10.4% for TIAC.

Comparison of the OAR absorbed doses obtained with DTK+OLINDA and with PLANET®Dose, LDM and DK, are presented in Table 7. Similarly, these results show that the mean difference and RMSD values are within 10 % for all organs except for spleen with a maximum RMSD value of 10.9%. For kidneys and spleen, the AD values obtained with PLANET®Dose are slightly but significantly higher ($p<0.05$).

The mean difference is 2.2% between the values calculated with LDM and DK from PLANET®Dose, similarly to the body phantom results. Values obtained with the LDM method are always higher than those obtained with the DK method. Fig. 4 illustrates the similarity of the AD distribution obtained for each organ using the two dosimetry workstations. Moreover, whatever the software used, liver presents the highest variability in the absorbed doses (b) with high values reaching around 16 Gy.

Concordance between platforms

For the all the 40 dosimetry evaluations, the estimated Lin's concordance correlation coefficient is 0.99 (95% CI 0.99; 0.99; R^2=0.9736) (Fig. 5a). This result suggests an excellent concordance between our current dosimetry method and PLANET®Dose. According to the Bland-Altman plot method (Fig. 5b, c, d),

the “bias” value (i.e. the mean of the AD differences between and PLANET®Dose and DTK+OLINDA) is -0.13 Gy for liver, 0.22 Gy for kidneys and 0.30 Gy for Spleen. Moreover, this approach estimated that the difference of AD values between methods ranges from -0.75 Gy to 0.49 Gy, from -0.20 Gy to 0.64 Gy and from -0.43 to 1.03 Gy for approximately 95% of the 40 liver, kidneys and spleen dosimetry analyses, respectively. For liver, the Bland-Altman analysis shows that the mean absolute dose differences increased when the dose gets higher (R^2 =0.5742).

Calculation method

Comparison of the mean AD obtained with PLANET®Dose LDM and DK and using the TIACs from PLANET®Dose uploaded on OLINDA/EXM® V1.0 (i.e. the reference in this comparison) is presented in Fig. 6 and Table 8. These results show that the mean relative difference and RMSD values are within 5 % for all organs except for spleen with a maximum RMSD value of 6.5%.

The estimated Lin’s concordance correlation coefficient is 1 (R^2=0.9966) (Fig. 7a). The “bias” value of the Bland-Altman plot analysis (i.e. the average of the differences between PLANET®Dose LDM and PLANET®Dose+OLINDA) is -0.16 Gy for liver, -0.06 Gy for kidneys and -0.04 Gy for Spleen. The difference of absorbed dose values between methods ranges from -0.57 Gy to 0.24 Gy, from -0.18 Gy to 0.06Gy and from -0.34 to 0.26 Gy for approximately 95% of the 40 liver, kidneys and spleen dosimetry analyses, respectively (Fig. 7b, c, d). For liver, the negative trend illustrate by the Bland-Altman analysis provides a R^2 value of 0.8358.

Discussion

Motivated by implementing central dosimetric processing for multicentric trials, our department acquired a vendor-neutral solution, PLANET®Dose, for dosimetry assessments. In order to preserve the experience and data acquired thus far with Dosimetry Toolkit® and OLINDA/EXM® V1.0, we needed to verify that the workstations would yield consistent results. Obviously, this can be achieved only if the same methodology is implemented in both platforms (38). Thus, our study, based on a fully 3D imaging protocol, evaluated dosimetric results obtained with the two dosimetry solutions, first using a body phantom and then in 21 patients undergoing [177Lu]Lu-DOTA-TATE treatment, representing a total of 40 dosimetry analysis.

First, due to the uncertainties associated with planar imaging, as described by Garkavij *et al.* (39), we implemented a fully SPECT/CT dosimetry protocol. In both cases, the reconstruction step was performed with the GE application “Preparation for Dosimetry Toolkit” because PLANET®Dose does not include this functionality. The latter accepts reconstructed data supplied by others workstations, unlike the “Dosimetry Toolkit” application. The used reconstruction parameters were determined in a previous study (29).

In a clinical dosimetry study, the preliminary step of calibration is crucial to obtain accurate activity quantification (40,41). As demonstrated in a multi-centre evaluation on phantoms (42) and also by Peters

et al. (43), a detailed calibration protocol is a real need to achieve accurate and reliable image quantification for multicentric studies. This was the goal of the recently completed joint European research project MRTdosimetry (44).

To evaluate the quantification accuracy, calibration methods with complex phantoms have been described. For example, Tran-Gia *et al*. (45) presented a 3D printed two-compartment kidney phantom. In our phantom-based study, as our first intention when we designed the clinical dosimetry protocol was to follow first line critical organ, we used large phantom containing a bottle as an object relatively close to the kidney.

To obtain the CF for each software package, the same methodology based on SPECT/CT imaging was followed. However, according to the General Electric's recommendations, a CF determined from a planar acquisition of a 15cm diameter petri dish partially filled with a solution of ^{177}Lu is preconized for DTK. Conversely, the calibration procedure is left to the physicist's discretion in PLANET®Dose. As described by Gustafsson et *al*.(46), SPECT segmentation is essential to determine the activity concentration. Different segmentation methods are proposed: manual, automatic or semi-automatic (from the technically very easy, such as fixed threshold, to the most complicated, such as the Fourier surface method). For our phantom-based study, we selected a fixed volume threshold method based on an automatically drawn isocontour around the bottle with a volume of 200 mL. This volume was segmented on the SPECT images acquired at the first time point and rigidly propagated to the others. This step is directly affected by the accuracy of the rigid registration of all SPECT/CT images (28,47,48). The CF obtained was in is the same order (within 10%) than that determined by Peters *et al*. (43) using a similar gamma camera model.

Moreover, CFs are expressed in counts.s^{-1}.MBq^{-1} by DTK and in Bq.count^{-1} by PLANET®Dose. This implies that the CF must be modified with the acquisition duration for PLANET®Dose. This also highlights a clear risk of mistake because of the absence of standardisation in the way calibration factors are introduced in dosimetry software. The crucial recommendation at this step is that the conditions used in clinical studies in terms of acquisition and reconstruction parameters have to be similar to those used for calibration.

We showed a negligible variation of CF values over time, from T=0 to 216h. This means that the same CF can be used for each time point. This observation is particularly interesting for DTK in which a single CF must be entered whereas a different CF can be used at each time point with PLANET®Dose.

With the body phantom, the mono-exponential function provided by each software package to fit time activity curves showed a slight difference especially at the Y-intercept probably due to the variation over time higher with the CF of PLANET®Dose. This could partly explain the difference of residence time obtained between platforms. Nevertheless, differences from the theoretical residence time below 6% are acceptable.

Concerning the AD estimation on phantom, OLINDA/EXM® V1.0 calculated the mean values by considering a kidney of 200 g. With PLANET®Dose, tissue density heterogeneities can be corrected using a method similar to that described by Dieudonne *et al*. (32). The DK method with density correction showed results close to those obtained with OLINDA/EXM® V1.0. The values calculated by OLINDA/EXM indicate that more than 98% of the absorbed dose comes from short-range beta particles of ^{177}Lu. Sandström *et al.* (49) demonstrated that the absorbed dose for kidneys is mainly due to the self-absorbed dose because only a minor proportion originates from the cross-absorbed dose due to gamma radiation from the surrounding organs. Our results showed a very small difference, below 2.5%, between LDM and DK for the phantom-based and the patient dosimetry evaluations. Therefore, as shown by Pasciak *et al.* (15) for selective internal radiotherapy with ^{90}Y, the LDM method is suitable also for ^{177}Lu (50–52).

In the patient study, the masses obtained with the two packages for liver were more similar than those obtained for smaller organs, such as kidneys and spleen, and the variability increased with the OAR decreasing size. The TIAC supplied by PLANET®Dose was generally higher than that calculated by DTK, as shown with the phantom-based study. Regarding AD, the Bland-Altman plots showed that the biases were quite low for all organs. The limits of agreement were rather tight with a maximum value of around 1 Gy for spleen. This issue has to be replaced in the clinical context. Moreover, the results for liver highlighted a trend that the absorbed dose from DTK+OLINDA became slightly higher than that calculated by PLANET®Dose when the absorbed dose increased. This trend is more pronounced for patients with liver metastasis i.e. high activity gradients within the liver.

A priori, for the voxel size considered, one can safely make the hypothesis that beta/electrons from ^{177}Lu are non-penetrating radiations. In that context, it doesn't really matter if the activity distribution is heterogeneous, or not (the average absorbed dose should be the same for OLINDA and PLANET®Dose). Then, one hypothesis could be that cross absorbed doses (from photons) may be different for heterogeneous vs. homogeneous activity distributions. However, the photon contribution to the liver absorbed dose is always low, and proportionally varies little with the volume. Another point to consider is the density (homogeneous for OLINDA vs. voxel-based and coming from the CT for PLANET®Dose). This may impact the absorbed dose calculation, but it's not clear at this stage to which extend. This certainly deserves an in depth analysis, probably involving Monte Carlo modelling as a ground truth, also to take into account the possible impact of local density corrections that may – or may not – be relevant (53).

PLANET®Dose calculates the AD at the voxel level and then rescales them at the organ level to provide the mean absorbed dose to the segmented organ. The software is not currently providing fully 3D dosimetry results (absorbed dose-volume histograms and isodose curves). In fact, voxel-based dosimetry is still a matter of debate (14–16,33,54–57), as it relies not only on radiation transport and absorbed dose calculation (which can be addressed voxel-wise with current algorithms), but also on activity (and cumulated activity) determination at the voxel level, which is much more challenging. Yet software exist that propose voxel-based absorbed dose determination (27,57).

The comparison of the dosimetric outcomes calculated by Planet®Dose and by OLINDA/EXM® V1.0, using the same TIACS provided by PLANET®Dose, showed that the calculation method has only a minor influence compared with all the previous steps (i.e. registration and segmentation). For accurate registration, position reproducibility during the four SPECT/CT acquisitions is crucial. Thus, patient set-up and immobilization devices are strongly recommended.

Our comparison methodology, using similar parameters in terms of registration, segmentation with constant volumes over time and mono-exponential function to fit the time activity curves, has some limitations. Indeed, using DTK, the segmented volume was maintained, but adjusted by translation or rotation at each time point when necessary. However, this step is not available in PLANET®Dose. To be as close as possible to the DTK approach, in PLANET®Dose we chose to perform an organ-based registration followed by rigid propagation. In their study, Grassi *et al*. (48) showed that absorbed doses to organs are significantly affected by the registration algorithm used. Indeed, due to respiratory motion during SPECT/CT and organ deformation, misregistration errors can happen. Thus, for some patients organ segmentation did not fully match at the other time points and the delineation was moved to organs with different density. This implies an important deviation when calculating the absorbed doses with density correction. For instance, in dosimetry analysis n°31, part of the spleen was moved to the left lung at other time points and the absorbed dose was overestimated because of the density correction. This observation could explain the important differences obtained for some patients and the observed significant differences. We are aware of the limitations of our methodology in this work, but we considered these deviations as clinically acceptable.

The concordance evaluation (Lin's coefficient value of 0.99) highlighted an excellent agreement between methods. Moreover, the dosimetry results obtained using PLANET®Dose (AD to liver, kidneys and spleen of 0.45 ± 0.50 Gy/GBq, 0.45 ± 0.13 Gy/GBq and 0.62 ± 0.17 Gy/GBq respectively) are in agreement with those of the literature (50).

As proposed by Gear *et al.* (58) in a practical guidance paper, the uncertainties at each step of the dosimetry analysis should be determined to express the accuracy of the dosimetry results. At the moment, PLANET®Dose offers an evaluation of the relative proportion of interpolation (between time points) and extrapolation (after last time point). Regardless of the goodness of the fit, this is a nice indication of the relevance of time sampling, but is not sufficient to characterise fully the uncertainties associated to the dosimetric workflow. Such study requires important developments and will be implemented in the future.

From a qualitative point of view, PLANET®Dose is a user-friendly commercial solution that proposes a wide range of tools for segmentation, and several analytic fit functions. The time necessary for a dosimetry analysis is significantly reduced. Therefore, considering the good agreement between our reference dosimetry method and PLANET®Dose, the concordance of the dosimetry results with the literature, the added value of this software in terms of easy contouring, wide choice of time activity curve fitting models, time saving, and the fact that the observed differences were explicable and clinically

acceptable, we think that the PLANET®Dose software can replace our current dosimetry package without any correction for dosimetry analysis. Since the results obtained are close enough, we can complete the migration and start investigating alternate methodological possibilities offered by PLANET®Dose, such as elastic registration and propagation, time integration activity with multiple exponentials, absorbed dose rates at the voxel level, dicom RT import and export of structures.

Conclusion

This comparative analysis validated PLANET®Dose, a software package available on the market, in clinical practice during peptide receptor radionuclide therapy with [177Lu]Lu-DOTA-TATE. Its potential can now be fully explored, particularly for the determination of tumour absorbed doses and for investigating absorbed dose-response correlations.

Abbreviations

AD: Absorbed Dose

CF: Calibration Factor

DK: Dose Kernel

DTK: Dosimetry Toolkit®

FOV: Field Of View

IDAC: Internal Dose Assessment by Computer

ICRP: Internal Commission on Radiological Protection

LDM: Local Deposition Method

MIRD: Medical Internal Radiation Dose

NETs: Neuroendocrine Tumours

OAR: Organ At Risk

OSEM: Ordered Subset Expectation Maximization

PRRT: Peptide Receptor Radionuclide Therapy

RMSD: Root Mean Square Deviation

SD: Standard Deviation

SPECT/CT: Single Photon Emission Computed Tomography / Computed Tomography

TACs: Time Activity Curves

TIA: Time Integrated Activity

TIAC: Time Integrated Activity Coefficient

Declarations

Ethics approval and consent to participate

All procedures performed in this study studies involving human participants were in accordance with the ethical standards of the institutional research committee.

Consent for publication

Consent has been obtained from participants to publish this work.

Availability of data and material

Please contact the author for data requests.

Competing interests

ED was invited in 2018 to attend an international meeting by AAA who sponsored registration fees and travel expenses. Otherwise, there are no potential conflicts of interest to disclose for any of the authors.

Funding

No funding was received.

Authors' contributions

LS, LP, DT, EMR carried out the phantom measurements, image reconstructions and data analysis. MB and ED participated to the design of the study. POK and ED were responsible of the patient acquisitions and treatments. LS was responsible of the dosimetry software implementation and performed patient dosimetry evaluations with LP. LS wrote the manuscript. All authors read and approved the final manuscript.

References

1. Chiesa C, Sjogreen Gleisner K, Flux G, Gear J, Walrand S, Bacher K, et al. The conflict between treatment optimization and registration of radiopharmaceuticals with fixed activity posology in oncological nuclear medicine therapy. Eur J Nucl Med Mol Imaging. 2017 Oct;44(11):1783–6.

2. Giammarile F, Muylle K, Delgado Bolton R, Kunikowska J, Haberkorn U, Oyen W. Dosimetry in clinical radionuclide therapy: the devil is in the detail. Eur J Nucl Med Mol Imaging. 2017 Nov;44(12):1–3.
3. Flux GD, Sjogreen Gleisner K, Chiesa C, Lassmann M, Chouin N, Gear J, et al. From fixed activities to personalized treatments in radionuclide therapy: lost in translation? Eur J Nucl Med Mol Imaging. 2018 Jan;45(1):152–4.
4. Huizing DMV, de Wit-van der Veen BJ, Verheij M, Stokkel MPM. Dosimetry methods and clinical applications in peptide receptor radionuclide therapy for neuroendocrine tumours: a literature review. EJNMMI Res [Internet]. 2018 Dec [cited 2018 Oct 21];8(1). Available from: https://ejnmmires.springeropen.com/articles/10.1186/s13550-018-0443-z
5. Strigari L, Konijnenberg M, Chiesa C, Bardies M, Du Y, Gleisner KS, et al. The evidence base for the use of internal dosimetry in the clinical practice of molecular radiotherapy. Eur J Nucl Med Mol Imaging. 2014 Oct;41(10):1976–88.
6. Council Directive 2013/59/Euratom of 5 December 2013 laying down basic safety standards for protection against the dangers arising from exposure to ionising radiation, and repealing Directives 89/618/Euratom, 90/641/Euratom, 96/29/Euratom, 97/43/Euratom and 2003/122/Euratom. :73.
7. Verburg FA, Giovanella L, Lassmann M, Chiesa C, Chouin N, Flux G. The “reset button” revisited: why high activity 131I therapy of advanced differentiated thyroid cancer after dosimetry is advantageous for patients. Eur J Nucl Med Mol Imaging. 2017 Jun;44(6):915–7.
8. Bolch WE, Eckerman KF, Sgouros G, Thomas SR. MIRD Pamphlet No. 21: A Generalized Schema for Radiopharmaceutical Dosimetry–Standardization of Nomenclature. J Nucl Med. 2009 Feb 17;50(3):477–84.
9. Bouchet LG, Bolch WE, Blanco HP, Wessels BW, Siegel JA, Rajon DA, et al. MIRD Pamphlet No. 19: Absorbed fractions and radionuclide S values for six age-dependent multiregion models of the kidney. J Nucl Med. 2003;44(7):1113–1147.
10. Snyder W, Ford M, Warner G, Watson S. MIRD Pamphlet No. 11: S, Absorbed Dose per Unit Cumulated Activity for Selected Radionuclides and Organs. N Y Soc Nucl Med. 1975;1–257.
11. Chauvin M, Borys D, Botta F, Bzowski P, Dabin J, Denis-Bacelar AM, et al. OpenDose: open access resources for nuclear medicine dosimetry. J Nucl Med. 2020 Mar 13;jnumed.119.240366.
12. Stabin MG, Sparks RB, Crowe E. OLINDA/EXM: the second-generation personal computer software for internal dose assessment in nuclear medicine. J Nucl Med. 2005;46(6):1023–1027.
13. Andersson M, Johansson L, Eckerman K, Mattsson S. IDAC-Dose 2.1, an internal dosimetry program for diagnostic nuclear medicine based on the ICRP adult reference voxel phantoms. EJNMMI Res. 2017 Dec;7(1):88.
14. Divoli A, Chiavassa S, Ferrer L, Barbet J, Flux GD, Bardies M. Effect of Patient Morphology on Dosimetric Calculations for Internal Irradiation as Assessed by Comparisons of Monte Carlo Versus Conventional Methodologies. J Nucl Med. 2009 Feb 1;50(2):316–23.
15. Pasciak AS, Bourgeois AC, Bradley YC. A Comparison of Techniques for 90Y PET/CT Image-Based Dosimetry Following Radioembolization with Resin Microspheres. Front Oncol [Internet]. 2014 May

22 [cited 2020 May 13];4. Available from: http://journal.frontiersin.org/article/10.3389/fonc.2014.00121/abstract

16. Giap HB, Macey DJ, Bayouth JE, Boyer. Validation of a dose-point kernel convolution technique for internal dosimetry. Phys Med Biol. 1995;40(3):365–81.
17. Giap HB, Macey DJ, Podoloff DA. Development of a SPECT-Based Three-Dimensional Treatment Planning System for Radioimmunotherapy. J Nucl Med. 1995;36(10):1885–94.
18. Bolch WE, Bouchet LG, Robertson JS, Wessels BW, Siegel JA, Howell RW, et al. MIRD Pamphlet No. 17: The Dosimetry of Nonuniform Activity Distributions_Radionuclide S Values at the Voxel Level. J Nucl Med. 1999;40(1).
19. Bardiès M, Ljungberg M. Monte-Carlo codes in radionuclide dosimetry. In: Dosimetry for Radionuclide Therapy. A Nicol, Editor. IPEM report 104, Institute of Physics and Engineering in Medicine.; 2011.
20. Sundlöv A, Gustafsson J, Brolin G, Mortensen N, Hermann R, Bernhardt P, et al. Feasibility of simplifying renal dosimetry in 177Lu peptide receptor radionuclide therapy. EJNMMI Phys [Internet]. 2018 Dec [cited 2018 Oct 21];5(1). Available from: https://ejnmmiphys.springeropen.com/articles/10.1186/s40658-018-0210-2
21. Marin G, Vanderlinden B, Karfis I, Guiot T, Wimana Z, Reynaert N, et al. A dosimetry procedure for organs-at-risk in 177Lu peptide receptor radionuclide therapy of patients with neuroendocrine tumours. Phys Med. 2018 Dec;56:41–9.
22. Del Prete M, Arsenault F, Saighi N, Zhao W, Buteau F-A, Celler A, et al. Accuracy and reproducibility of simplified QSPECT dosimetry for personalized 177Lu-octreotate PRRT. EJNMMI Phys. 2018 Dec;5(1):25.
23. Johnson TK, McClure D, McCourt S. MABDOSE II: Validation of a general purpose dose estimation code. Med Phys. 1999 Jul;26(7):1396–403.
24. Gardin I, Bouchet LG, Assié K, Caron J, Lisbona A, Ferrer L, et al. Voxeldose: A Computer Program for 3-D Dose Calculation in Therapeutic Nuclear Medicine. Cancer Biother Radiopharm. 2003 Feb;18(1):109-15.
25. Grimes J, Uribe C, Celler A. JADA: A graphical user interface for comprehensive internal dose assessment in nuclear medicine: A GUI for comprehensive internal dose assessment. Med Phys. 2013 Jun 19;40(7):072501.
26. Kletting P, Schimmel S, Hänscheid H, Luster M, Fernández M, Nosske D, et al. The NUKDOS software for treatment planning in molecular radiotherapy. Z Für Med Phys. 2015 Sep;25(3):264–74.
27. Li T, Zhu L, Lu Z, Song N, Lin K-H, Mok GSP. BIGDOSE: software for 3D personalized targeted radionuclide therapy dosimetry. Quant Imaging Med Surg. 2020 Jan;10(1):160–70.
28. Mora-Ramirez E, Santoro L, Cassol E, Ocampo-Ramos JC, Clayton N, Kayal G, et al. Comparison of commercial dosimetric software platforms in patients treated with ^{177} Lu-DOTATATE for peptide receptor radionuclide therapy. Med Phys. 2020 Jul 31;mp.14375.

29. Santoro L, Mora-Ramirez E, Trauchessec D, Chouaf S, Eustache P, Pouget J-P, et al. Implementation of patient dosimetry in the clinical practice after targeted radiotherapy using [177Lu-[DOTA0, Tyr3]-octreotate. EJNMMI Res. 2018 Dec;8(1):103.
30. GE Healthcare. Organ Dose estimates for Radio-Isotope Therapy treatment planning purposes. Dosimetry toolkit package. White Paper. 2011.
31. Kupitz D, Wetz C, Wissel H, Wedel F, Apostolova I, Wallbaum T, et al. Software-assisted dosimetry in peptide receptor radionuclide therapy with 177Lutetium-DOTATATE for various imaging scenarios. Mosley RL, editor. PLOS ONE. 2017 Nov 6;12(11):e0187570.
32. Dieudonne A, Hobbs RF, Lebtahi R, Maurel F, Baechler S, Wahl RL, et al. Study of the Impact of Tissue Density Heterogeneities on 3-Dimensional Abdominal Dosimetry: Comparison Between Dose Kernel Convolution and Direct Monte Carlo Methods. J Nucl Med. 2013 Feb 1;54(2):236–43.
33. Dieudonne A, Hobbs RF, Bolch WE, Sgouros G, Gardin I. Fine-Resolution Voxel S Values for Constructing Absorbed Dose Distributions at Variable Voxel Size. J Nucl Med. 2010 Oct 1;51(10):1600–7.
34. Kondev FG. Lu-177_comments on evaluation of decay data for beta- decay. 2002.
35. Simpkin DJ. Radiation Interactions and Internal Dosimetry in Nuclear Medicine. 1999;19(1):13.
36. Lin LI-K. A Concordance Correlation Coefficient to Evaluate Reproducibility. Biometrics. 1989 Mar;45(1):255.
37. Altman DG, Bland JM. Measurement in Medicine: The Analysis of Method Comparison Studies. The Statistician. 1983 Sep;32(3):307.
38. Huizing DMV, Peters SMB, Versleijen MWJ, Martens E, Verheij M, Sinaasappel M, et al. A head-to-head comparison between two commercial software packages for hybrid dosimetry after peptide receptor radionuclide therapy. EJNMMI Phys. 2020 Dec;7(1):36.
39. Garkavij M, Nickel M, Sjögreen-Gleisner K, Ljungberg M, Ohlsson T, Wingårdh K, et al. 177Lu-[DOTA0,Tyr3] octreotate therapy in patients with disseminated neuroendocrine tumors: Analysis of dosimetry with impact on future therapeutic strategy. Cancer. 2010 Feb 15;116(S4):1084–92.
40. Zhao W, Esquinas PL, Hou X, Uribe CF, Gonzalez M, Beauregard J-M, et al. Determination of gamma camera calibration factors for quantitation of therapeutic radioisotopes. EJNMMI Phys [Internet]. 2018 Dec [cited 2018 Oct 22];5(1). Available from: https://ejnmmiphys.springeropen.com/articles/10.1186/s40658-018-0208-9
41. Uribe CF, Esquinas PL, Tanguay J, Gonzalez M, Gaudin E, Beauregard J-M, et al. Accuracy of 177Lu activity quantification in SPECT imaging: a phantom study. EJNMMI Phys [Internet]. 2017 Dec [cited 2017 Sep 12];4(1). Available from: http://ejnmmiphys.springeropen.com/articles/10.1186/s40658-016-0170-3
42. Zimmerman BE, Grošev D, Buvat I, Coca Pérez MA, Frey EC, Green A, et al. Multi-centre evaluation of accuracy and reproducibility of planar and SPECT image quantification: An IAEA phantom study. Z Für Med Phys. 2017 Jun;27(2):98–112.

43. Peters SMB, Meyer Viol SL, van der Werf NR, de Jong N, van Velden FHP, Meeuwis A, et al. Variability in lutetium-177 SPECT quantification between different state-of-the-art SPECT/CT systems. EJNMMI Phys. 2020 Dec;7(1):9.
44. Lassmann M, Eberlein U. The relevance of dosimetry in precision medicine. J Nucl Med. 2018 Jul 12;jnumed.117.206649.
45. Tran-Gia J, Lassmann M. Optimizing Image Quantification for ^{177} Lu SPECT/CT Based on a 3D Printed 2-Compartment Kidney Phantom. J Nucl Med. 2018 Apr;59(4):616–24.
46. Gustafsson J, Sundlöv A, Sjögreen Gleisner K. SPECT image segmentation for estimation of tumour volume and activity concentration in 177Lu-DOTATATE radionuclide therapy. EJNMMI Res. 2017 Dec;7(1):18.
47. Grassi E, Fioroni F, Ferri V, Mezzenga E, Sarti MA, Paulus T, et al. Quantitative comparison between the commercial software STRATOS® by Philips and a homemade software for voxel-dosimetry in radiopeptide therapy. Phys Med. 2015 Feb;31(1):72–9.
48. Grassi E, Fioroni F, Berenato S, Patterson N, Ferri V, Braglia L, et al. Effect of image registration on 3D absorbed dose calculations in 177 Lu-DOTATOC peptide receptor radionuclide therapy. Phys Med. 2018 Jan;45:177–85.
49. Sandström M, Ilan E, Karlberg A, Johansson S, Freedman N, Garske-Román U. Method dependence, observer variability and kidney volumes in radiation dosimetry of 177Lu-DOTATATE therapy in patients with neuroendocrine tumours. EJNMMI Phys. 2015 Dec;2(1):24.
50. Sandstrom M, Garske-Roman U, Granberg D, Johansson S, Widstrom C, Eriksson B, et al. Individualized Dosimetry of Kidney and Bone Marrow in Patients Undergoing 177Lu-DOTA-Octreotate Treatment. J Nucl Med. 2013 Jan 1;54(1):33–41.
51. Ilan E, Sandstrom M, Wassberg C, Sundin A, Garske-Roman U, Eriksson B, et al. Dose Response of Pancreatic Neuroendocrine Tumors Treated with Peptide Receptor Radionuclide Therapy Using 177Lu-DOTATATE. J Nucl Med. 2015 Feb 1;56(2):177–82.
52. Jahn U, Ilan E, Sandström M, Garske-Román U, Lubberink M, Sundin A. ^{177}Lu-DOTATATE Peptide Receptor Radionuclide Therapy: Dose Response in Small Intestinal Neuroendocrine Tumors. Neuroendocrinology. 2020;110(7–8):662–70.
53. Hippeläinen E, Tenhunen M, Sohlberg A. Fast voxel-level dosimetry for ^{177} Lu labelled peptide treatments. Phys Med Biol. 2015 Sep 7;60(17):6685–700.
54. Chiesa C, Bardiès M, Zaidi H. Voxel-based dosimetry is superior to mean absorbed dose approach for establishing dose-effect relationship in targeted radionuclide therapy. Med Phys. 2019 Dec;46(12):5403–6.
55. Grimes J, Celler A. Comparison of internal dose estimates obtained using organ-level, voxel S value, and Monte Carlo techniques: Comparison of internal dose estimate techniques. Med Phys. 2014 Aug 14;41(9):092501.

56. Tran-Gia J, Salas-Ramirez M, Lassmann M. What You See Is Not What You Get: On the Accuracy of Voxel-Based Dosimetry in Molecular Radiotherapy. J Nucl Med. 2020 Aug;61(8):1178–86.
57. Hippeläinen ET, Tenhunen MJ, Mäenpää HO, Heikkonen JJ, Sohlberg AO. Dosimetry software Hermes Internal Radiation Dosimetry: from quantitative image reconstruction to voxel-level absorbed dose distribution. Nucl Med Commun. 2017 May;38(5):357–65.
58. Gear JI, Cox MG, Gustafsson J, Gleisner KS, Murray I, Glatting G, et al. EANM practical guidance on uncertainty analysis for molecular radiotherapy absorbed dose calculations. Eur J Nucl Med Mol Imaging [Internet]. 2018 Sep 14 [cited 2018 Oct 12]; Available from: http://link.springer.com/10.1007/s00259-018-4136-7

Tables

Due to technical limitations, the tables are provided in the Supplementary Files section.

Figures

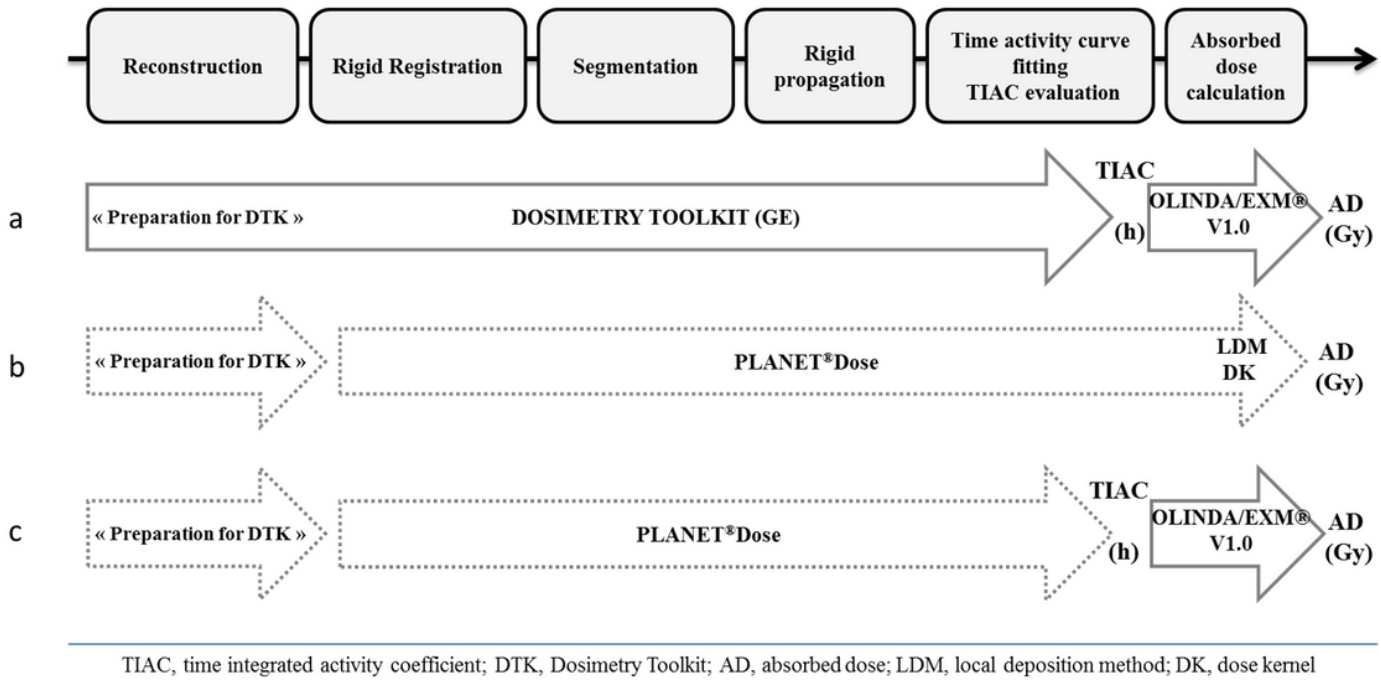

Figure 1

Dosimetry workflow for the phantom study and in patients using the reference dosimetry approach DTK+OLINDA (a) and the new workstation PLANET Dose with LDM and DK methods (b). The configuration (c): PLANET®Dose + OLINDA was used to evaluate independently the absorbed dose calculation methods.

a

b

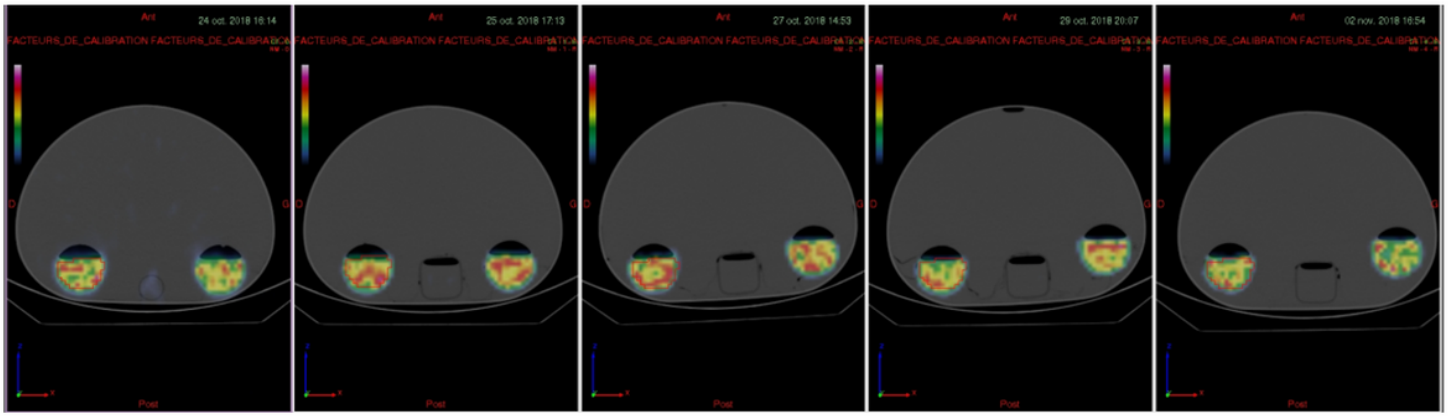

Figure 2

Dosimetry Toolkit (a) and PLANET®Dose interfaces (b) with the NEMA IEC body phantom (Body Phantom NU2-2001/2007) imaging, containing two bottles of 250 mL filled with 200 mL of [177Lu]Lu-DOTA-TATE. Only one of the two inserts was segmented.

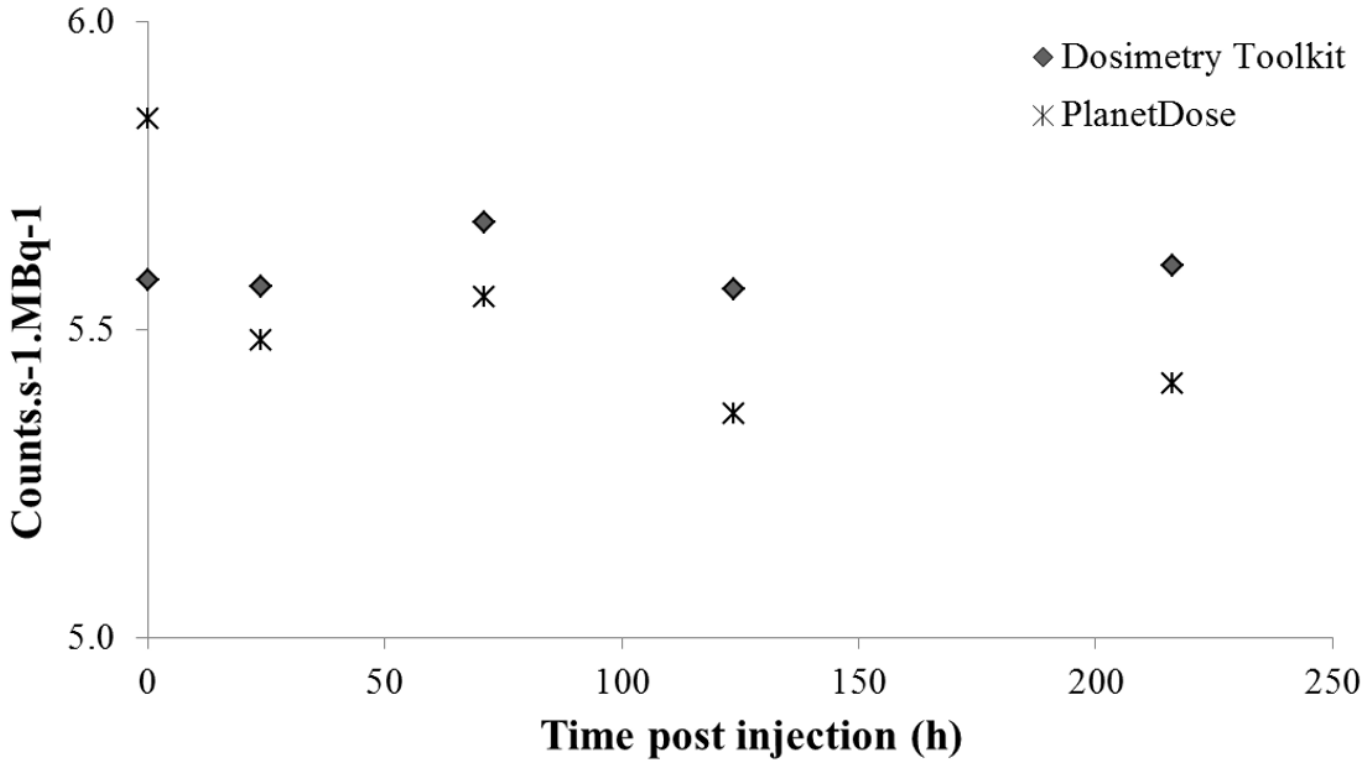

Figure 3

Variation of the SPECT CF values over time after injection obtained with Dosimetry Toolkit (a) and PLANET®Dose (b).

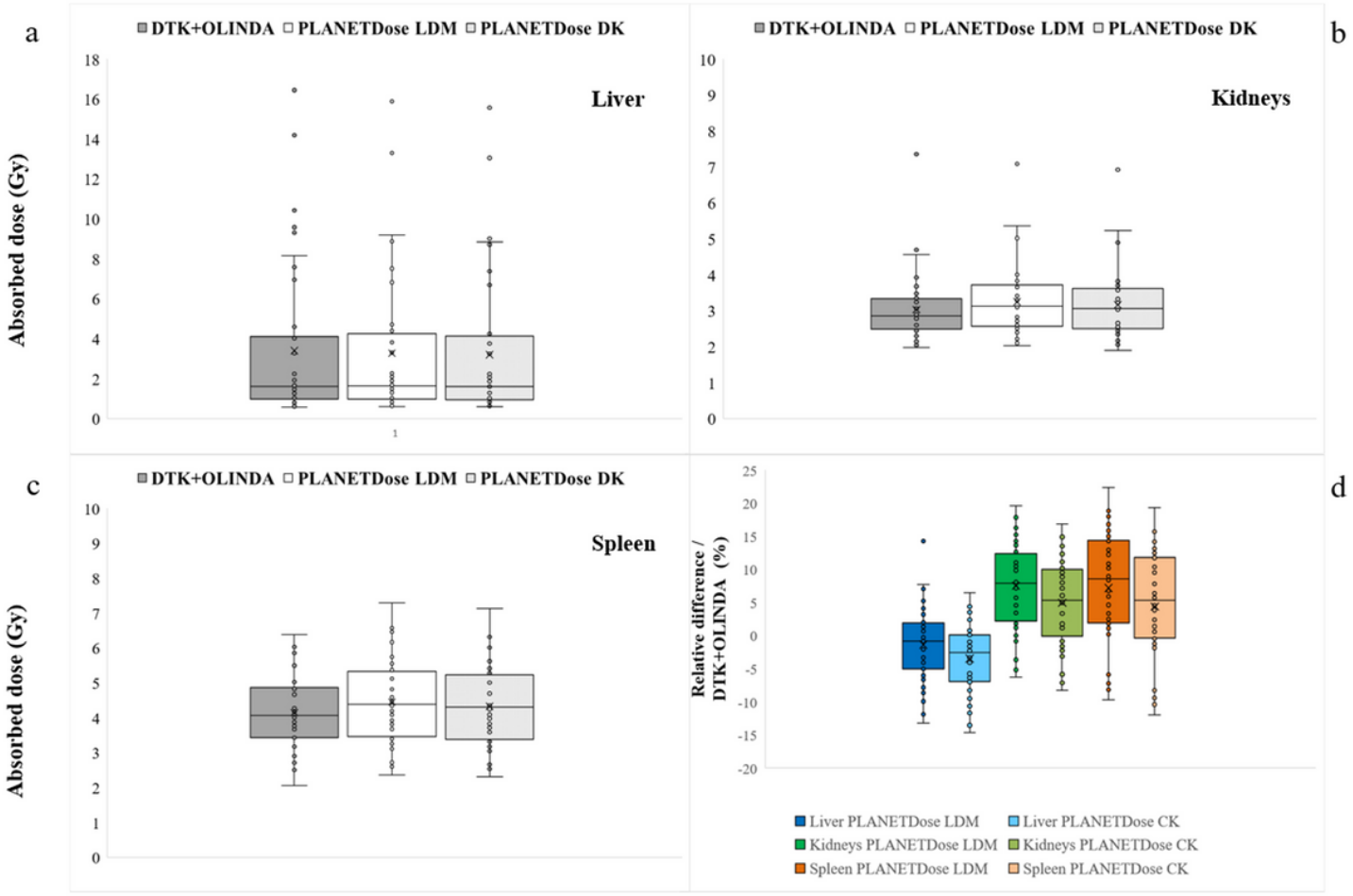

Figure 4

Box-and-whisker plots of absorbed dose to liver (a), kidneys (b) and spleen (c) calculated using DTK+OLINDA and the PLANET®Dose workstation. Relative differences of absorbed doses between PLANET®Dose and DTK+OLINDA are presented on box-and-whisker plots (d).

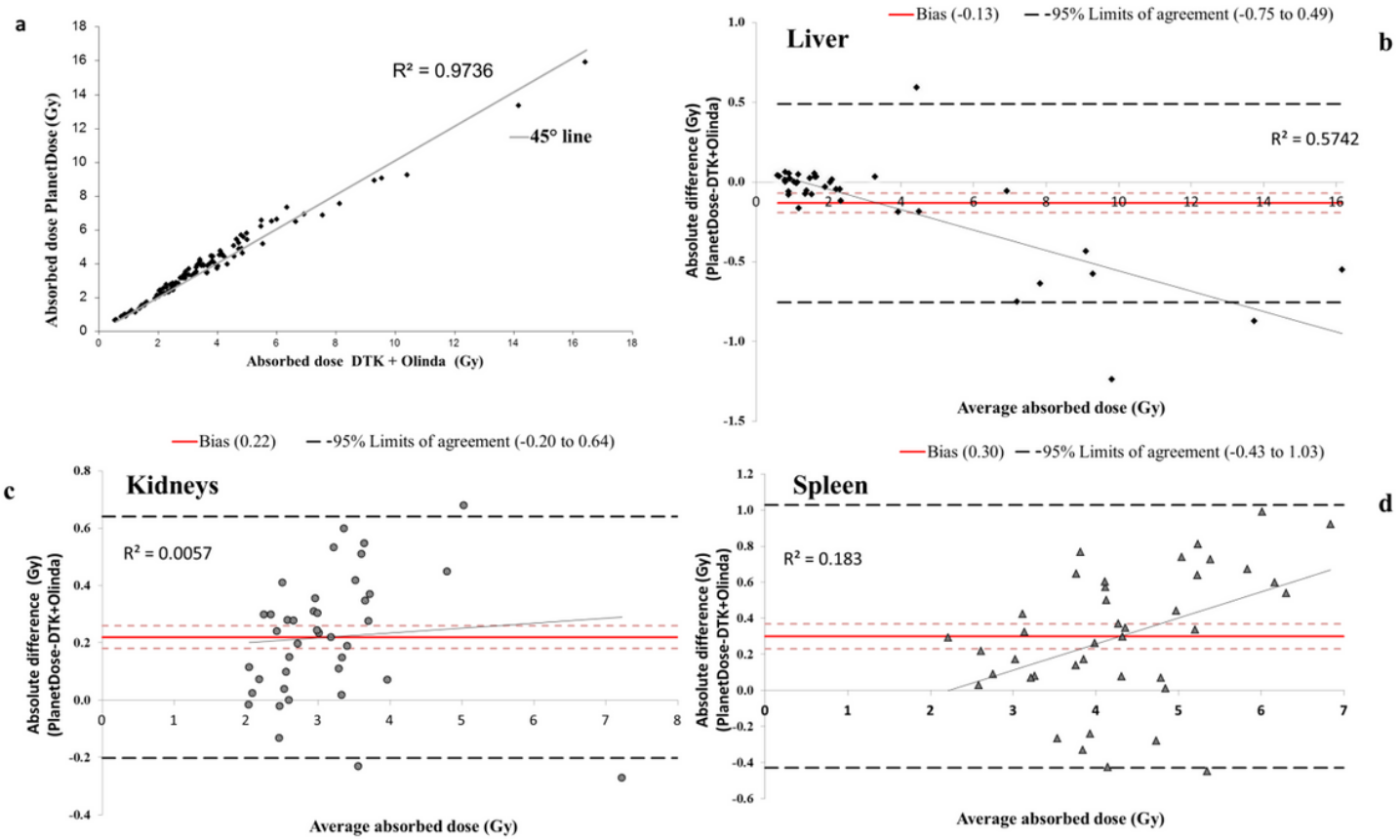

Figure 5

Dispersion around the 45° line of the absorbed dose pairs obtained with DTK+OLINDA and PLANET®Dose LDM with density correction for all organs combined (a). Bland-Altman plots of absorbed doses to liver (b), kidneys (c) and spleen (d) calculated with DTK+OLINDA and PLANET®Dose LDM with density correction.

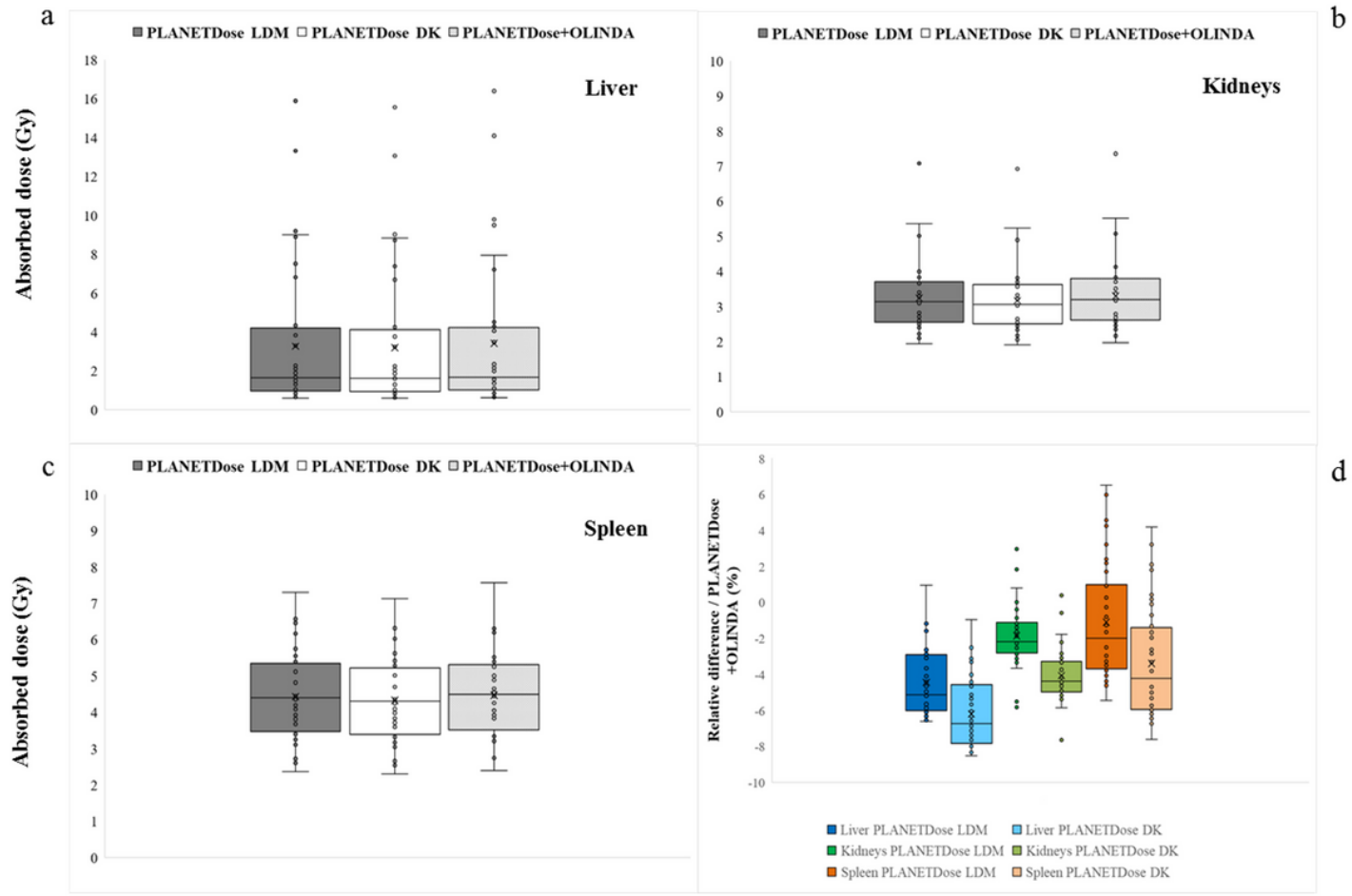

Figure 6

Box-and-whisker plots of absorbed dose to liver (a), kidneys (b) and spleen (c) calculated using PLANET®Dose workstation and PLANET®Dose + OLINDA. Relative differences of absorbed doses between PLANET®Dose workstation and PLANET®Dose + OLINDA are presented on box-and-whisker plots (d).

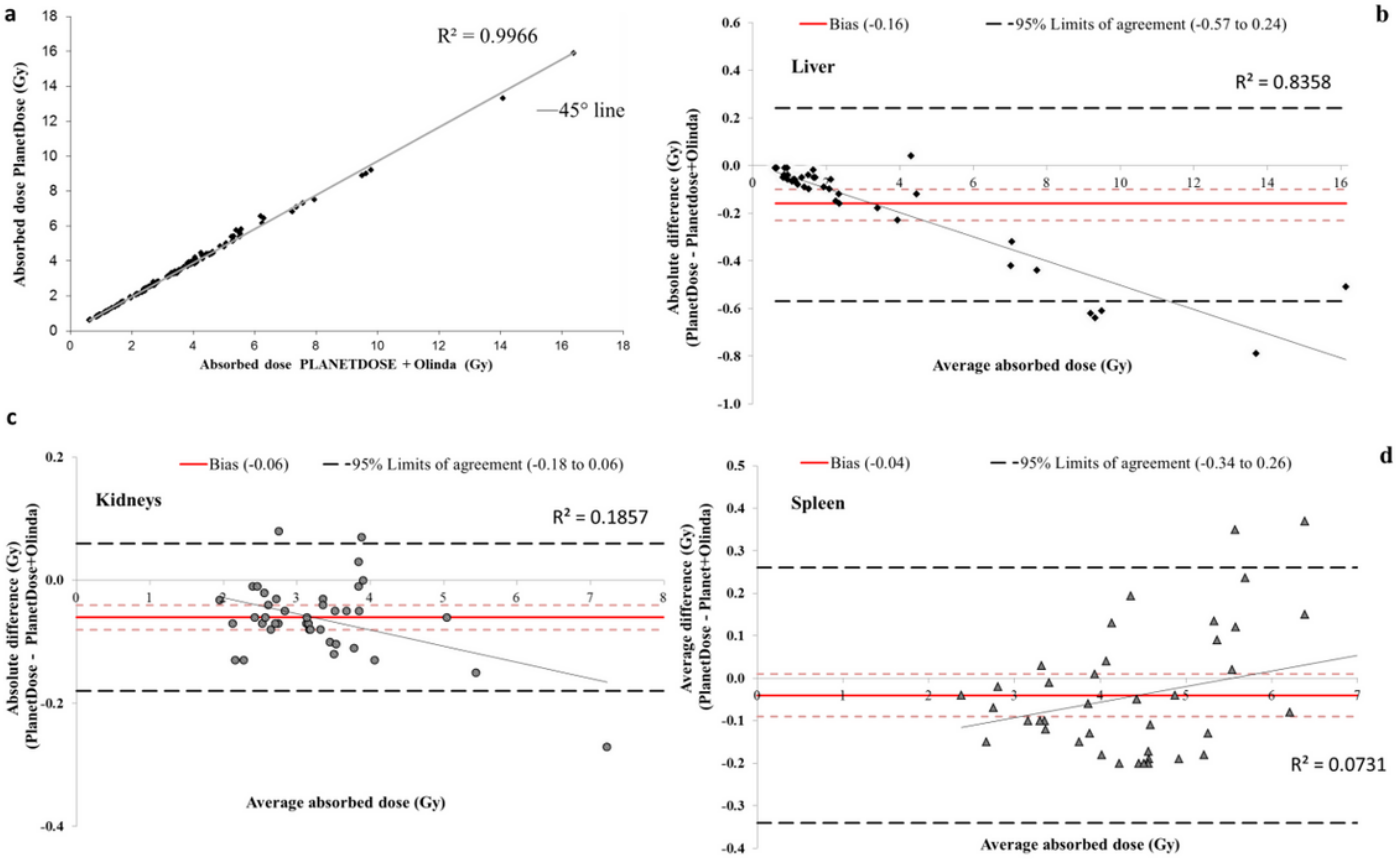

Figure 7

Dispersion around the 45° line of the absorbed dose pairs obtained with PLANET+OLINDA and PLANET®Dose LDM with density correction for all organs combined (a). Bland-Altman plots of absorbed doses to liver (b), kidneys (c) and spleen (d) calculated with PLANET+OLINDA and PLANET®Dose LDM with density correction.

Supplementary Files

This is a list of supplementary files associated with this preprint. Click to download.

- Table1.docx
- Table3.docx
- Table2.docx
- Table4.docx
- Table5.docx
- Table6.docx
- Table7.docx
- Table8.docx